Optics Communications 283 (2010) 2829–2834

Contents lists available at ScienceDirect

Optics Communications

journal homepage: www.elsevier.com/locate/optcom

10 Gb/s broadband silicon electro-optic absorption modulator

Ali W. Elshaari *, Stefan F. Preble

Microsystems Engineering, Kate Gleason College of Engineering, Rochester Institute of Technology, Rochester, NY 14623, USA

ARTICLE INFO

Article history:
Received 9 December 2009
Received in revised form 22 March 2010
Accepted 22 March 2010

ABSTRACT

Here we propose a design for a novel broadband silicon electro-optic absorption modulator. The device is simply a 100 μm long silicon waveguide with a Schottky diode integrated in it. Modulation is achieved through free-carrier absorption, not interference effects, enabling operation over the entire bandwidth of the waveguide. The high overlap between the modulated carrier density and the optical mode enables high speed (>10 Gb/s), small footprint and modulation depths of ~4.6 dB.

1. Introduction

Nanophotonic circuits have great promise for overcoming the limitations of electronic interconnects, especially in applications that require high bandwidths, low powers and low noise. Crystalline silicon is now the preferred platform for building these nanophotonic devices because of its low intrinsic loss at telecommunication wavelengths, the compatibility with CMOS processes, and high index contrast.

One of the most important components of a nanophotonic communication system is a fast electro-optic modulator, which takes in a DC optical input signal and switches it on/off using a high data-rate electronic signal. Modulation is achieved by inducing a change in the phase or the intensity of the light, using a refractive index change or an absorption change, respectively. In silicon the free-carrier plasma dispersion (FCPD) effect can achieve both [1–4]. However, in all recently demonstrated electro-optic devices the FCPD has been relatively small, requiring either very large photonic devices or devices that leverage resonant effects to increase the sensitivity to small refractive index changes. However, using resonant effects come with a tradeoff — the bandwidth of the device dramatically decreases. This is especially true for modulators based on micro-resonators, such as rings or discs [1,3–5]. The bandwidth of these resonators is so small that they are extremely sensitive to temperate variations, and very small fabrication imperfections. To overcome this limitation, high powered and complicated compensation techniques are required to precisely set and maintain the resonant wavelengths of all of the devices on the chip [6]. Alternatively, Mach–Zehnder interferometer modulators have been demonstrated which significantly increase the optical bandwidth [7,8]. Although the system described in [7] achieves modulation speeds up to 30 Gb/s, it is relatively large (~3 mm long) due to the small overlap of the light with the carrier modulation. While sub-micron waveguides can reduce the overall size of the modulator [8], the overall photonic structure has a more complex structure than the one proposed here. In addition, both modulators in [7,8] suffer from significant free-carrier absorption due to the overlap of the optical mode with doped regions and/or injected carrier densities. In contrast, here we utilize the inherent free-carrier absorption present in FCPD modulators to realize a broadband, high speed, compact, electro-optic modulator.

Here we propose a very simple modulator that solves the problems encountered with the previous structures. This modulator is fundamentally different from all the other recently demonstrated modulators in that it relies on the absorption change in silicon instead of the refractive index change. Therefore, it does not require a resonance or interference effect, it just requires a simple short waveguide. Since light is just absorbed, the device inherently operates over the entire bandwidth of the waveguide where the mode has sufficient confinement (more than 100 nm bandwidth centered at wavelength of 1.55 μm). As a result of this the device has minimal sensitivity to process variations which allows the integration of multiple matched devices on the same chip without the use of any complicated structures for wavelength insensitivity [12].

The modulator is realized by integrating Schottky diodes into the waveguide to control the free-carrier density. Schottky diodes have a significant advantage over traditional PN/PIN diodes because they are majority carrier devices that operate with very low turn on voltages, and are very fast [3]. The proposed design has a very high overlap between the optical mode and the large modulated carrier density, which results in a large change in the optical absorption over a short length. This is in stark contrast to previously demonstrated electro-absorption modulators based on free carriers in silicon that were inherently slow and large in size due to their reliance on PN/PIN diodes [9,10]. In addition, while germanium-on-silicon modulators based on the Stark effect are showing initial promise they inherently require a significantly more complicated integration and fabrication scheme than the device proposed here [11]. In the following sections the

* Corresponding author.
E-mail address: awe2048@rit.edu (A.W. Elshaari).

0030-4018/$ – see front matter © 2010 Elsevier B.V. All rights reserved.
doi:10.1016/j.optcom.2010.03.048

design of our simple modulator is presented with models to monitor the behavior of the device and the transient response for fast switching operation.

2. Device design

The modulator structure is simply a 100 μm long silicon-on-insulator single mode waveguide. The waveguide dimensions are 250 nm in height, including a thin 50 nm rib, and 450 nm in width, as seen in Fig. 1. The middle region of the waveguide is lightly doped to 10^{16} cm^{-3} with P type dopant (Boron). This concentration as will be seen in our simulations results in a low OFF state loss, and a wide depletion region due to the internal voltage difference between the Schottky contact and the doped silicon. The ribs on the sides of the waveguide are heavily P doped to 10^{19} cm^{-3}. When the device is turned ON holes from these ribs are injected into the middle region where the optical mode resides. The device has three terminals, two ohmic aluminum contacts connected to the heavily doped ribs 700 nm away from the waveguide in order to minimize the loss, and a single 50-nm wide aluminum Schottky contact (Gate) connected to the top of the waveguide. The contact resistance in the modeling is assumed to be 2 kΩ which matches previous analytical models [17] and experimental results [1]. While the positioning of the gate on top of the waveguide and the P+ doped regions do induce some insertion loss, the total insertion loss of the device is only 2.98 dB. While a larger metal region will be needed to make electrical contact to this gate, a modest via of size 200×200 nm placed anywhere along the top of the waveguide would introduce an additional attenuation of only 3%. The electrical arrangement of our modulator has a significant advantage over commonly used PN/PIN based approaches such as [1,8] in that the carriers are forced to flow directly through the center of the waveguide where the optical mode resides, ensuring optimal light and free-carrier concentration overlap.

3. Device modeling

The device is simulated using a two-dimensional simulation package ATLAS from SILVACO [13]. This program simulates internal physics and device characteristics of semiconductor devices by solving Poisson's equation and the charge continuity equations for electrons and holes numerically. The software allows a complete statistical approach (Fermi–Dirac statistics) when heavily doped regions are considered [14]. The suitability of this device modeling package to analyze electro-optic modulators in SOI waveguides has been demonstrated by several other authors [14–17]. Several physical models were used to accurately predict the behavior of the device such as field and concentration dependant mobility, Shockley–Read–Hall (SRH) recombination model, Auger recombination model and band narrowing for the regions with high carrier concentration. A surface recombination model is also used to account for the semiconductor/insulator interface recombination. The carrier interface recombination velocity and the surface recombination velocity are taken as 8000 cm/s each [17], while the electrons and hole lifetimes in bulk silicon are taken as 3 μs and 10 μs respectively [17]. The highly doped are assumed to have an abrupt junction [15] for simplicity. This has a negligible effect on the carrier transport phenomena of the devices compared to realistic Gaussian profiles with 35 nm normal deviation [16]. The design of these devices allows for the junctions to have a fast lateral decay rate when they are realized using low keV ion implantation. The top Schottky contact is made from aluminum which has a work function of 4.1 eV [3]. The ohmic tunneling contacts are also made from aluminum but are connected to the heavily doped P regions. The behavior of the aluminum contact (i.e. whether it is ohmic or Schottky) simply depends on the doping level/work function of the silicon it is attached to. In practice a short low-temperature anneal (400–500 °C) may be required to form a good quality Schottky contact.

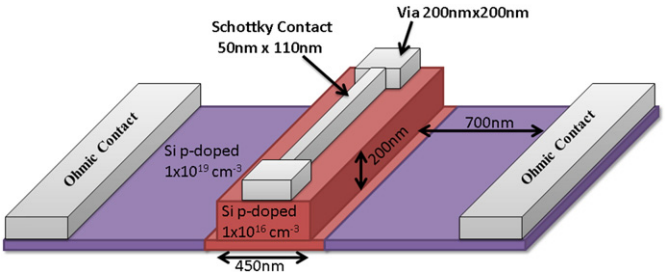

Fig. 1. Cross-section of the Schottky diode waveguide modulator. The device consists of a lightly doped center region where the light is confined. A 50 nm wide Schottky contact is attached to the top. A 50 nm highly doped rib is at the bottom of the waveguide where ohmic contacts (700 nm away from the center region) are attached. The waveguide is embedded in silicon dioxide. The device length is 100 μm (not to scale).

A finite difference mode solver was used to calculate the complex effective index of the waveguide in order to characterize the wave propagation and loss. Taking into account all of the doped regions, carrier concentrations [18] and metal contacts (analyzed with Drude model) the complex effective index of the mode obtained from the optical simulation is used to calculate the transmittance of an optical signal through the modulator using the following equations:

$$T = e^{(-\alpha \cdot L)} \tag{1}$$

$$\alpha = \frac{n_g}{\mathrm{Re}(n_{\mathrm{eff}})}\left({}^{4\pi}/_{\lambda}\right)\cdot \mathrm{Im}(n_{\mathrm{eff}}) \tag{2}$$

where α denotes the power absorption coefficient, L is the length of the device, n_g is the group index of the waveguide, $\mathrm{Re}(n_{\mathrm{eff}})$ is the real part of the complex effective index, λ is the wavelength of operation and $\mathrm{Im}(n_{\mathrm{eff}})$ is the imaginary part of the effective index. The first term of Eq. (2) essentially accounts for the slowed propagation of the light due to the reduced group velocity of the mode in the waveguide. This term is important in nanosized waveguides because the group index is significantly larger than the effective index of the mode [19]. The group index is calculated using the mode solver and the well known equation:

$$n_g = n_{\mathrm{eff}} - \lambda \frac{dn_{\mathrm{eff}}}{d\lambda} \tag{3}$$

4. Results and discussion

Fig. 2 shows the calculated hole carrier distribution profile when the device is OFF. Taking this off-state carrier concentration into account and all other sources of optical losses, such as the metal contacts, a characterization of the optical mode was made to measure the effective index and intrinsic loss of the device.

Fig. 3 shows the calculated mode profile for the magnetic and electric fields of the TE mode. It is seen that most of the light resides

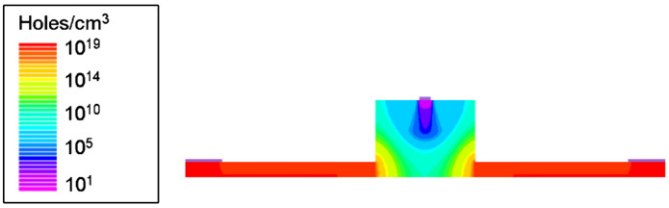

Fig. 2. The hole carrier concentration density profile in the devices off-state. It is seen that there is a very low carrier concentration in the center waveguide region where the light resides.

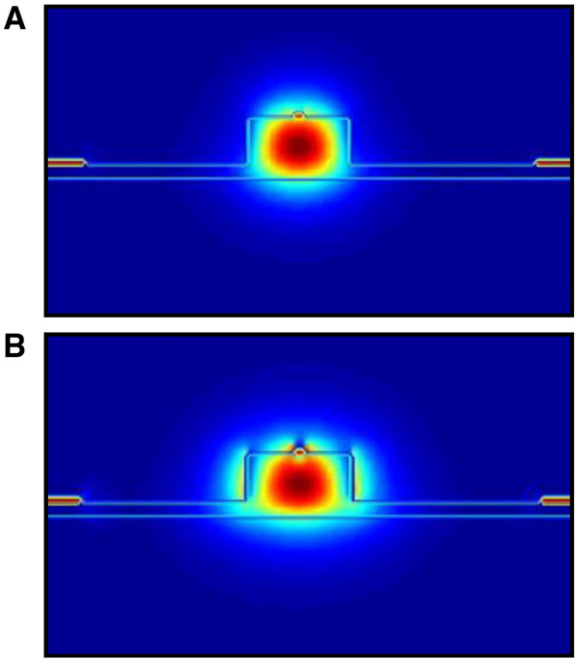

Fig. 3. The (A) vertical magnetic field intensity and (B) horizontal electric field for the TE mode of the waveguide.

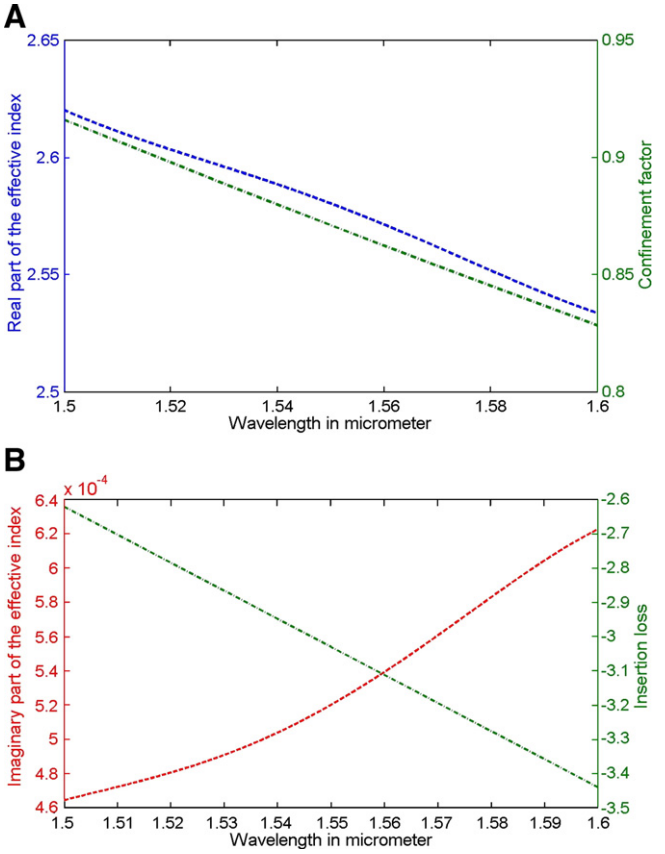

Fig. 4. (A) Real part of the effective index (blue) and the amount of power confined in the central silicon region where the carrier concentration is modulated (green). (B) Imaginary part of the effective index (red) and the total insertion loss of a 100 μm long device (green).

in the central region with a very low carrier concentration, and consequently low initial loss.

The dependence of the real and imaginary part of the effective index on wavelength is shown in Fig. 4 taking into count the material dispersion of silicon, oxide, and aluminum [21]. At the operating wavelength of 1550 nm the real part of the effective index is found to be 2.5817, and the imaginary part is 5.17E−04. The absorption coefficient is related to the imaginary part of the refractive index by Eq. (2), which then can be used to calculate the transmission of the device using Eq. (1). From this we find that the device has an insertion loss of only 2.98 dB for a device length of 100 μm ($n_g = 3.996$) even though there is metal directly on top of the waveguide. In addition, the insertion loss only varies by 0.78 dB over a 100 nm bandwidth as plotted on the right *y*-axis of Fig. 4B, which demonstrates the very broadband nature of the device. Unfortunately losses are much higher for the other polarization state but with the recent demonstration of polarization rotators on a chip, it is possible to have an entire chip operating at a single polarization [20].

As mentioned earlier modulation in the optical signal is achieved through a change in absorption by injecting/extracting a high carrier density into the optical mode. The carrier concentration is modulated by applying a forward or reverse bias to the gate while connecting the other two ohmic terminals to ground. Here we use a maximum reverse bias voltage of +1.25 V, and a minimum forward voltage of −1.25 V. Reverse bias (forward bias) occurs with a positive (negative) voltage because the device is P doped. We can see the low hole concentration in the waveguide region under reverse bias in Fig. 5A, and the very high hole concentration in the forward biasing operation in Fig. 5B. It is seen that there is a very large change in carrier concentration (10^{19}) exactly where the optical mode resides. Such a large carrier concentration change results in a very large change of the absorption coefficient of the device, which is directly leveraged to modulate light in the waveguide.

The change in the absorption coefficient is calculated using the change in the electron and hole concentration with the following equation [18]:

$$\Delta\alpha_{fc} = \left[8.5 \times 10^{-18} \times \Delta N + 6 \times 10^{-18} \times \Delta P\right] \quad (4)$$

where $\Delta\alpha_{fc}$ is the change in the free-carrier absorption coefficient per unit length (cm^{-1}), and ΔN and ΔP are the change in the electron and holes density per cm^3, respectively. The carrier distribution in Fig. 5A represents the reverse biased condition (OFF state) where the operating voltage is below the threshold of the device and there is low carrier concentration where the optical mode resides. Although the carrier density changes with space (10^9 cm^{-3} to 10^{14} cm^{-3} over the whole waveguide) it has a negligible effect on the free carriers loss at this state according to Eq. (4) $\Delta\alpha_{fc} \sim 0$. Once a current is established in the device (forward biased junction, voltages >0.5 V) the carrier

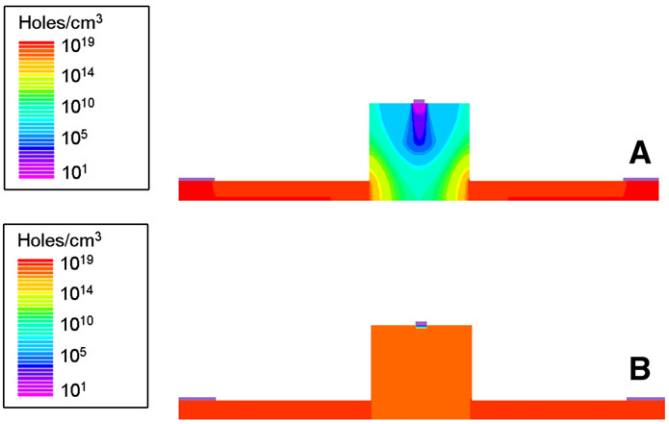

Fig. 5. The log of the hole density profile with a (A) 1.25 V reverse bias and (B) a 1.25 V forward bias.

concentration is extremely uniform (10^{15} cm^{-3}) over the entire active region of the mode due to the small waveguide dimensions and the vertical design of the contacts as seen in Fig. 5B. Therefore, as a simplification it can be assumed that the carrier concentration is a constant over this entire region in the forward bias operation and the approximate change in the modes absorption coefficient is given by [19]:

$$\Delta\alpha = \frac{n_g}{n_b}\gamma_{fc}\Delta\alpha_{fc} \tag{5}$$

where $\Delta\alpha$ is the change in modes absorption coefficient, n_g is the group index, n_b is the bulk index of silicon (3.46) and γ_{fc} is the free-carrier spatial confinement factor of the mode which accounts for the amount of light that interacts with the modulated free-carrier concentration (i.e. in the center) and is given by Eq. (6) [19]. Due to the strong overlap of the light with the free carriers we find that this confinement factor is 87%

$$\gamma_{fc} = \frac{\iint_{center} \varepsilon|E|^2 dxdy}{\iint_{\infty} \varepsilon|E|^2 dxdy}. \tag{6}$$

Since $n_g/n_b = 1.15$, we find that $\Delta\alpha = 1.003\Delta\alpha_{fc}$, which allows us to simplify that the change in the absorption of the mode is approximately just given by Eq. (4). From this we can directly calculate the change in transmission from the modulated carrier concentration using Eq. (1). Lastly, the right y-axis of Fig. 4A shows the change in the confinement factor given by Eq. (6) as a function of wavelength. We see that it varies by only 9% and the approximation we make here is approximately valid over more than 100 nm bandwidth.

Fig. 6 shows the negative of the input signal applied to the gate (the signal is flipped to conform with normal convention that positive voltages correspond to a forward-biases) in order to demonstrate the high speed of the proposed modulator. It is seen that the forward bias voltage is pre-emphasized with a −4 V short voltage pulse and then reduced to −1.25 V. This pre-emphasis technique has been commonly used in the forward biasing of previously demonstrated ring resonator and Mach–Zehnder PIN modulators [8,17]. Pre-emphasis effectively increases the power of the high frequency components of the input signal which consequently increases the speed that the effective carrier concentration is injected. Fig. 7 shows the optical response of the 100 μm long waveguide device to the voltage signal applied in Fig. 5A (calculated using Eqs. (1) and (4)). It is seen that the modulation depth of the device is more than 65% (~4.6 dB). A larger modulation depth can be achieved with a tradeoff in insertion loss as explained below.

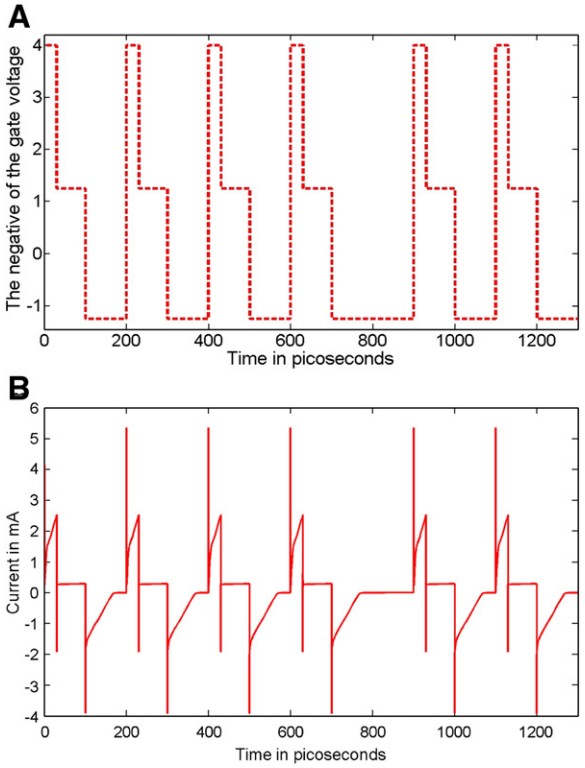

Fig. 6. 10 Gb/s gate voltage and current applied to the Schottky modulator device. Note that voltage is flipped for convention that higher voltages refer to forward bias (but is actually negative since this device is actuated by holes).

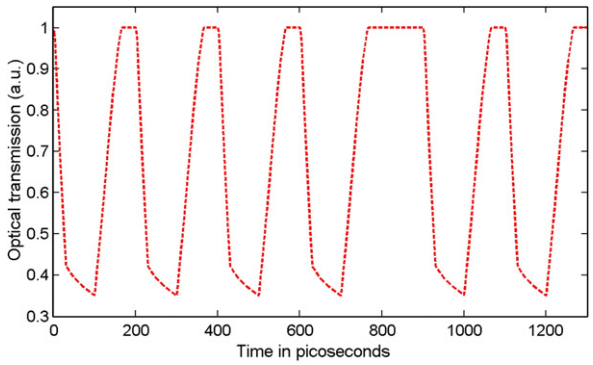

Fig. 7. Optical response of the Schottky modulator to the gate signal applied in Fig. 6. It is seen that a modulation depth of >4.6 dB is achieved at a bit-rate of 10 Gb/s.

Fig. 8 gives a closer look at the response of the carriers over one period of the voltage input signal. The device reaches steady state OFF transmission (high carrier concentration) in only 30 ps from the ON state (low carrier concentration), and only takes 60 ps to go from OFF to back ON. The high speed of the device and large majority carrier concentration change (10^{19}) are directly enabled by the use of a Schottky junction which works by thermionic emission of majority carriers over the barrier created by the unequal work functions between a metal–semiconductor interface. This is in stark contrast to the operation of PN/PIN devices, which are limited by relatively small and slow minority carrier concentration processes, which inherently require ultrasensitive and complex interference based optical devices in order to achieve significant modulation [1,2,7,8]. The fast transition times of the Schottky device enable operation at speeds of 10 Gb/s and our modeling indicates that even faster switching is possible with a tradeoff of higher insertion loss. It is important to note that our device does not have any RC constant limitations due to the low capacitance of Schottky diodes in comparison with PIN diodes. The depletion capacitance of the entire device was calculated to be 50 fF compared

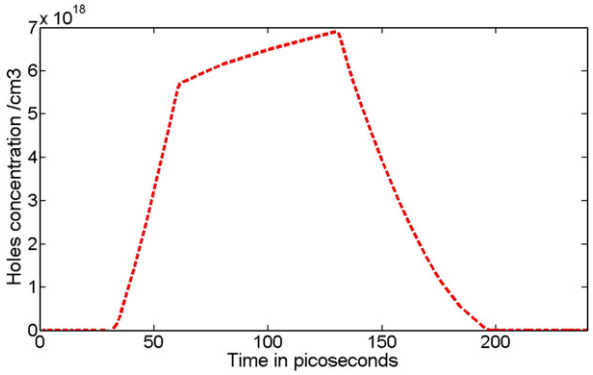

Fig. 8. Hole concentration over one period of an applied gate signal. It is seen that the rise time of the concentration is only 30 ps and the fall time is 60 ps.

to larger values in PIN structures of 200 fF [8]. In order to accurately characterize the RC time constant of the system, the resistivity of the top aluminum contact (thickness of 110 nm) was determined based on theoretical models and experimental measurements in [22]. Usually metal contacts such as copper with a line width approaching the electron mean free path (EMFP) (39 nm at room temperature) experience a strong increase in resistivity that is attributed to surface and grain boundary scattering. This phenomenon can be studied in different metals using Fuchs–Sondheimer (FS) surface scattering and Mayadas–Shatzkes (MS) grain boundary scattering models. However, this increase in the resistance is less pronounced in aluminum contacts with the same size due to the small EMFP of 15 nm [22]. The sizes of the contacts used (gate 50 nm × 110 nm) in the design are much larger than the EMFP size limit, which makes the resistivity approaches the bulk values of 2.66 μΩ cm for aluminum. Based on the resistivity value we can easily calculate the input resistance to be 245 Ω (Eq. (7)) looking from the gate to the drain and the source. Although the current in the modulator flows vertically from the gate to the source and drain there is some current conduction along the length of the device through the gate contacts due to the finite conductivity of aluminum when voltages are connected to the vias (gate region shown in Fig. 1) while the drain and source are grounded. This creates an equipotential point in the center of the gate. Lastly, the input resistance can be further reduced using multiple vias with a tradeoff of more insertion loss.

$$R = \rho \frac{L}{A} \tag{7}$$

Where ρ is the resistivity, L is the contact length (50 μm) and A is the contact area (110 nm × 50 nm). The time constant of the device can be calculated as follows

$$\tau = RC = 50^{-15} \times 245 = 12.75\,\text{picoseconds}. \tag{8}$$

Finally the cut-off frequency of the device is calculated from the RC time constant

$$f = \frac{1}{2\pi RC} = \frac{1}{2\pi \times 12.75\,\text{ps}} = 12.5\,\text{GHz}. \tag{9}$$

The cut-off frequency is higher than the operation speed of the device of 10 GHz. This shows that the device has no RC speed limitations.

As explained earlier there is an inherit tradeoff between modulation depth and insertion loss in the proposed device. As the device is made longer the off-state insertion loss from the metal gate and highly doped regions increases as seen in Fig. 9. However, the modulation depth is increased due to the additional free-carrier absorption from the majority carriers. These trade-offs can be varied slightly by modifying the device geometry (wider gate contact, with a tradeoff in additional loss), but this also results in a change in the operating speed and maximum carrier concentration of the device. One additional source of loss in the system which has a negligible effect on the performance is scattering loss. It mainly consists of an inherent waveguide scattering loss and mode mismatch loss through coupling light to the modulator. The first type comes from the rough side-walls of the waveguide due to the etching process. A typical value for the attenuation is 3 dB/cm [23] which comes to an insertion loss of ~0.03 dB for the total length of the modulator (100 μm). The second type of scattering loss comes from the small mode mismatch at the input/output ports of the modulator with the silicon waveguide. This is due to the presence of contact vias and aluminum gate on the top of the waveguide. We performed mode mismatch calculations and estimated the insertion loss from this effect to be ~0.2 dB. In summary the total insertion loss of the device including all the scattering loss mechanisms metal loss, carrier losses, scattering loss, and mode mismatch loss is approximately 3.25 dB.

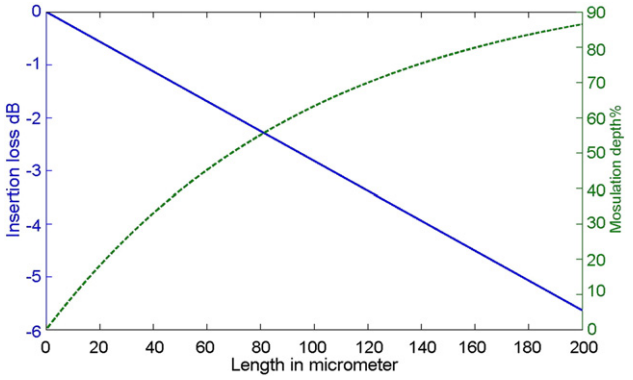

Fig. 9. Insertion loss and modulation depth of the device as a function of device length.

Lastly, although the device draws more current than PIN devices (consequently more power), its high switching speed and ultra-high continuous bandwidth (more than 100 nm) make it a vital component in broadband optical communication systems. Hundreds of channels from different systems can be processed in the same device because of the absence of any wavelength dependence. While large ring resonators (radius > 100 μm) have been demonstrated to switch many ITU channels simultaneously, they would require a similar switching power as used here due to their inherently large circumference of ~1 mm [24]. However, they would still require the use of complicated temperature compensation schemes. Another advantage is the robustness of the design to fabrication imperfections; because the device simply consists of a straight waveguide it can be built in any length without having precise dimensions and even looped as spirals to reduce the overall footprint on chip. In terms of modulation there are no complexities of matching resonances or using feedback techniques for stable operation through fixing the operating point as required in resonant or interference structures.

5. Conclusion

Here we've proposed a design for a simple broadband silicon electro-optic modulator based on free-carrier absorption in a silicon-on-insulator waveguide. The device is capable of at least 10 Gb/s operation and with further tuning of the device geometry, such as waveguide dimensions and the Schottky gate width, the device can be tuned for higher speed operation or lower loss. We are actively working towards fabricating and demonstrating this device experimentally.

Acknowledgements

We would like to acknowledge insightful discussions with Karthik Narayanan and Dr. James Moon on device design. We thank Dr. Christina Manolatou of Cornell University for the finite difference mode solver. Computational resources were provided by Research Computing, Rochester Institute of Technology. The authors acknowledge support from the Microsystems Engineering program and the Lobozzo Optics Laboratory.

References

[1] Q. Xu, B. Schmidt, S. Pradhan, M. Lipson, Nature 435 (2005) 325.
[2] B. Schmidt, Q. Xu, J. Shakya, S. Manipatruni, M. Lipson, Opt. Express 15 (2007) 3140.
[3] N.K. Hon, Zhou Linjie, A.W. Poon, CLEO, May 2007.
[4] M.R. Watts, D.C. Trotter, R.W. Young, OFC Postdeadline, 2008.
[5] Po. Dong, Shirong Liao, Dazeng Feng, Hong Liang, Dawei Zheng, Roshanak Shafiiha, Cheng-Chih Kung, Wei Qian, Guoliang Li, Xuezhe Zheng, Ashok V. Krishnamoorthy, Mehdi Asghari, Opt. Express 17 (2009) 22484.

[6] S. Manipatruni, R.K. Dokania, B. Schmidt, J. Shakya, A.B. Apsel, M. Lipson, Opt. Lett. 33 (2008) 19.
[7] Ansheng Liu, Ling Liao, Doron Rubin, Hat Nguyen, Berkehan Ciftcioglu, Yoel Chetrit, Nahum Izhaky, Mario Paniccia, Opt. Express 15 (2007) 660.
[8] William M. Green, Michael J. Rooks, Lidija Sekaric, Yurii A. Vlasov, Opt. Express 15 (2007) 17106.
[9] D.W. Zheng, B.T. Smith, M. Asghari, Opt. Express 16 (2008) 16754.
[10] G.V. Treyz, P.G. May, J.-M. Halbout, IEEE Electron Device Lett. 276 (1991) 12.
[11] Jifeng Liu, Mark Beals, Andrew Pomerene, Sarah Bernardis, Rong Sun, Jing Cheng, Lionel C. Kimerling, Jurgen Michel, Nature Photonics 2 (437) (2008) 433.
[12] Yurii Vlasov, William M.J. Green, Fengnian Xia, Nature Photonics 2 (2008) 4.
[13] http://www.silvaco.com/.
[14] C.A. Barrios, IEEE J. Lightwave Technol. 24 (2006) 2146.
[15] C. Angulo Barrios, V.R. Almeida, M. Lipson, IEEE J. Lightwave Technol. 21 (2003) 1089.
[16] C.A. Barrios, V.R. Almeida, R. Panepucci, M. Lipson, IEEE J. Lightwave Technol. 21 (2003) 2332.
[17] S. Manipatruni, Q. Xu, B. Schmidt, J. Shakya, M. Lipson, Lasers and Electro-Optics Society, LEOS, 2007.
[18] R.A. Soref, B.R. Bennett, IEEE J. Quant. Electron. QE-23 (1987) 123.
[19] Jacob T. Robinson, Kyle Preston, Oskar Painter, Michal Lipson, Opt. Express 16 (2008) 16659.
[20] Tymon Barwicz, Michael R. Watts, Miloš A. Popović, Peter T. Rakich, Luciano Socci, Franz X. Kärtner, Erich P. Ippen1, Henry I. Smith, Nature Photonics 1 (2006) 57.
[21] B.H.A. Saleh, M.C. Teich, Fundamentals of Photonics2nd Ed., Wiley, 2007.
[22] W. Zhang, S.H. Brongersma, O. Richard, B. Brijs, R. Palmans, L. Froyen, K. Maex, Microelectron. Eng. 76 (2004) 146.
[23] Yurii Vlasov, Sharee McNab, Opt. Express 12 (2004) 1622.
[24] B.G. Lee, A. Biberman, P. Dong, M. Lipson, K. Bergman, IEEE Photon. Technol. Lett. 20 (2008) 767.